

No real advantage of photon subtraction and displacement in continuous variable measurement device independent quantum key distribution

Chandan Kumar,^{1,*} Sarbani Chatterjee,^{1,†} and Arvind^{1,‡}

¹*Department of Physical Sciences, Indian Institute of Science Education and Research Mohali, Sector 81 SAS Nagar, Punjab 140306 India.*

We critically analyse the role of single photon subtraction (SPS) and displacement in improving the performance of continuous variable measurement device independent quantum key distribution (CV-MDI-QKD). We consider CV-MDI-QKD with resource states generated by SPS on a displaced two-mode squeezed vacuum state. Optimizing the secret key rate with state parameters reveals that implementing SPS yields no benefits in improving the loss tolerance of CV-MDI-QKD. Additionally, we find that displacement too is not useful in improving the performance of CV-MDI-QKD. While our result is in contradistinction with the widely held belief in the field regarding the utility of SPS and displacement in CV-MDI-QKD, it also calls for a re-examination of the role of non-Gaussian operations in increasing the efficiency of various quantum information processing protocols.

Introduction.— Quantum key distribution (QKD) is a quantum communication process whereby two distant parties, Alice and Bob, establish a shared secret key in the presence of Eve, a hostile third party eavesdropper [1–3]. The security of such protocols is guaranteed by the fundamental laws of quantum physics [2]. Depending upon the quantum systems involved, QKD protocols are primarily classified into discrete variable (DV) QKD [4–7] and continuous variable (CV) QKD protocols [8–14]. Due to its potential advantages, CV-QKD has attracted significant interest, leading to the rapid growth of the field, and several CV-QKD techniques have been theoretically studied and experimentally demonstrated in the last two decades [3].

Although the theoretical foundations of CV-QKD protocols have been shown to be unconditionally secure, their actual implementation may be compromised if the assumption of ideal devices cannot be fulfilled. This might be exploited by an eavesdropper to covertly glean information about the secret key. This problem was addressed by the device-independent QKD (DI-QKD) protocol, which does away with all presumptions about the different devices involved [15, 16]. However, the low secret key rate and short transmission distance render the DI-QKD protocol impracticable. Subsequently, measurement-device-independent QKD (MDI-QKD) protocols were proposed for DV systems, to remove assumptions on the detectors [17, 18]. Thereafter, the concept of MDI was extended to the CV framework [19–21].

While Gaussian states and operations have been at the heart of CV quantum information processing [13, 22, 23], there has been a shift in attention towards non-Gaussian states and operations [24]. This can be largely owed to the fact that non-Gaussianity is essential for entanglement distillation [25–27] and CV quantum compu-

tation [28, 29]. Non-Gaussian operations have been shown to improve performance of quantum teleportation [30–32], quantum sensing [33, 34] and QKD [35–37]. For instance, single photon subtraction (SPS) has been shown to enhance the tolerance to channel losses in CV-MDI-QKD, thereby extending the maximum transmission distance [38–40]. More specifically, Ref. [38] generated an SPS two-mode squeezed vacuum (TMSV) state and showed that tolerance to channel losses can be enhanced. Subsequently, Refs. [39, 40] employed SPS coupled with displacement by implementing SPS on a two-mode squeezed coherent (TMSC) state in CV-MDI-QKD and showed that tolerance to channel losses can be further enhanced.

While Refs. [39, 40] analysed the secret key rate at a fixed value of the variance, transmissivity and displacement parameters of the SPS-TMSC state, the Ref. [38] considered the variance to be fixed and optimized the secret key rate over transmissivity. In the present work, we consider the optimization of the secret key rate over all the state parameters aiming to enhance the performance of the SPS-based CV-MDI-QKD protocol further and to save on resources.

Surprisingly, our study reveals that SPS and displacement do not provide any advantage in the optimal situation. Further, the numerical results shown in Ref. [38] corresponding to SPS-TMSV state based CV-MDI-QKD are incorrect, invalidating their conclusion claiming enhanced channel loss tolerance. Similarly, channel loss tolerance enhancement demonstrated for SPS-TMSC state based CV-MDI-QKD in Refs. [39, 40] was an artifact of working at high variances.

Our findings have broader implications, while they directly impacts studies involving the utility of SPS and displacement in CV-MDI-QKD protocols [41–43] it also calls for optimization studies to assess the utility of SPS, and displacement in other CV-QKD protocols including entanglement-based CV-QKD protocol [36], entanglement in the middle CV-QKD protocol [35] and virtual post selection based CV-QKD protocols [37].

The calculation of the covariance matrix of the SPS-

* chandan.quantum@gmail.com

† mp18015@iisermohali.ac.in

‡ arvind@iisermohali.ac.in

TMSC state required for the evaluation of the secret key rate in the Hilbert space approach or the Wigner function approach [39] is challenging and cumbersome. Instead, in this work, we employ the Wigner characteristic function formalism [23, 44] for convenience and the derivation is provided in the companion paper.

SPS-TMSC state based CV-MDI-QKD.— We recapitulate the SPS-TMSC state based CV-MDI-QKD protocol here [20, 39]. While the schematic for the protocol is shown in Fig. 1, the steps involved in the process of generating a secret key between Alice and Bob under this protocol are outlined below:

Step 1. Alice prepares the required TMSC state by the action of the two-mode squeezing operator $S_{12}(r) = \exp[r(\hat{a}_{A_1}^\dagger \hat{a}_{A_2}^\dagger - \hat{a}_{A_1} \hat{a}_{A_2})]$ on the coherent state:

$$|\psi\rangle_{A_1 A_2} = S_{12}(r) D_1(d) D_2(d) |00\rangle, \quad (1)$$

where both the modes are displaced along their respective \hat{q} -quadrature by an amount d , *i.e.*, $D_i(d) = \exp[d(\hat{a}_{A_i}^\dagger - \hat{a}_{A_i})]$. The squeezing parameter r is related to the variance V of the quadrature operators via the relation $V = \cosh(2r)$ [13, 14]. We obtain the TMSV state by setting $d = 0$ in Eq. (1).

Step 2. Alice transfers the mode A_2 to Fred for the implementation of the SPS operation. In order to facilitate entanglement swapping, the photon-subtracted mode A'_2 is transferred to Charlie over a quantum channel of length L_{AC} .

Step 3. Bob prepares a TMSC state of modes B_1 and B_2 , similar to the one prepared by Alice (with an associated variance V and displacement d) and transfers the latter mode to Charlie through a quantum channel of length L_{BC} .

Step 4: Using a beam splitter, Charlie mixes the received modes A'_2 and B_2 , and subsequently subjects the output modes, labelled as C and D , to homodyne measurements of \hat{q} and \hat{p} operators, respectively. The measurement outcomes are denoted as $\{Q_C, P_D\}$, respectively, and are declared by Charlie.

Step 5: On the basis of these declared outcomes by Charlie, Bob subjects his retained mode B_1 , to an appropriate displacement operation $\hat{D}(g(Q_C + iP_D))$, with g being a gain factor. Subsequently, the label of the retained mode is changed to B'_1 , and marks the completion of the entanglement swapping process, with the final scenario of the modes A_1 and B'_1 being entangled. Alice and Bob carry out heterodyne measurements on their retained modes to obtain the correlated outcomes, $\{Q_A, P_A\}$ and $\{Q_B, P_B\}$ respectively.

Step 6: In the final step classical data post-processing including information reconciliation (reverse reconciliation) and privacy amplification are carried out to obtain the secret key.

Secret key rate.— We model the channel between Alice and Charlie as a noisy channel characterized by transmissivity T_A and excess noise $\varepsilon_A^{\text{th}}$, while the one between Bob and Charlie is characterized by transmissivity T_B and excess noise $\varepsilon_B^{\text{th}}$.

The relation between the transmissivity T_A and transmission distance L_{AC} of the quantum channel between Alice and Charlie is related by $T_A = 10^{-wL_{AC}/10}$, where w is the attenuation factor in decibels per kilometer (dB/km) [45]. In this work, we consider $w = 0.16$ dB/km [46]. Further, we approximate the excess noise using a linear fitting as $\varepsilon_A^{\text{th}} = 19.09 \times 10^{-5} + 6.13 \times 10^{-5} \times L_{AC}$ based on the experimental values of Ref. [46]. Since the CV-MDI-QKD protocol involves two quantum channels, Eve can implement a correlated two-mode coherent Gaussian attack, where quantum correlations are injected in both quantum channels, known as the two-mode attack [19, 47]. However, in a practical scenario, if the two quantum channels originate from distinct directions, the correlation between these two channels should be less. Furthermore, generating quantum correlations into both channels poses technical challenges for Eve. Hence, we confine our study to two Markovian memoryless Gaussian quantum channels that operate independently without mutual interaction. In such a scenario, the attack by Eve reduces to a one-mode collective Gaussian attack [21, 38].

Assuming that all of Bob's operations, except for the heterodyne detection, are not trustworthy, the CV-MDI-QKD protocol described above transforms into a one-way QKD protocol that employs heterodyne detection [20, 48, 49]. We emphasize that the secret key rate for the equivalent one-way QKD protocol is less than or equal to the original protocol. We use this one-way QKD protocol to calculate a bound on the secret key rate for convenience in calculation [50].

Let T and ε^{th} denote the transmissivity and excess noise of the quantum channel in equivalent one-way QKD protocol. The transmissivity T can be written as $T = \frac{g^2}{2} T_A$ where g is the gain of the displacement operation performed by Bob [20]. Further, the optimized excess noise can be expressed as [20]

$$\varepsilon^{\text{th}} = \frac{T_B}{T_A} (\varepsilon_B^{\text{th}} - 2) + \varepsilon_A^{\text{th}} + \frac{2}{T_A}. \quad (2)$$

We can write the total channel-added noise as $\chi_{\text{ch}} = \frac{1-T}{T} + \varepsilon^{\text{th}}$. Let I_{AB} denote the mutual information between Alice and Bob and χ_{BE} denotes the Holevo bound between Bob and Eve, then the secret key rate of the CV-MDI-QKD protocol is given by

$$K = P_{\text{SPS}} (\beta I_{AB} - \chi_{BE}), \quad (3)$$

where P_{SPS} is the success probability of SPS operation and β is the reconciliation efficiency. The analytical expression for P_{SPS} is provided in Refs. [39, 40]. The details of the calculations of mutual information and Holevo bound are provided in Appendix A. Further, the computation of the covariance matrix for the SPS-TMSC state, essential for determining the secret key rate in either the Hilbert space or Wigner function approach [39], presents significant challenges and complexities. However, in this study, we opt for the Wigner characteristic function for-

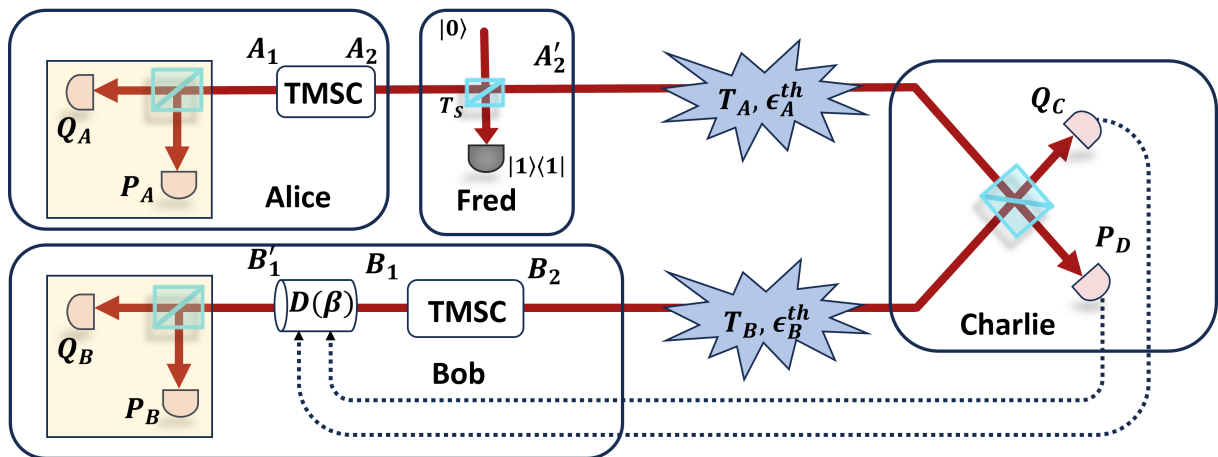


FIG. 1. Schematic illustration of SPS-TMSC state based CV-MDI-QKD. The SPS operation is implemented by Fred using a beam splitter of transmissivity T_S and a single photon detector.

malism for its practicality and ease of use. The derivation of the Wigner characteristic function and the covariance matrix in concise form are provided in the companion paper. The total transmission distance turns out to be $L = L_{AC} + L_{BC}$. In this article, we will consider the scenario when Bob and Charlie are together ($L_{BC} = 0$ *i.e.*, $T_B = 1$) as it renders a high transmission distance. The advantage of working with the key rate given in Eq. (3) is that one can span over various parameter regimes beginning from TMSV to SPS-TMSC, compare and also optimize the secret key rate.

Parameter optimization. – In Ref. [38], the secret key was optimized with respect to transmissivity¹. To motivate the need to consider the optimization of the secret key rate over variance, we first analyze the TMSV state based CV-MDI-QKD and show that variance can be optimized to maximize the secret key rate. To this end, we plot the secret key rate as a function of variance at different fixed transmission distances and show the results in Fig. 2.

We observe that the secret key rate does not increase with variance; instead, there is an optimal variance that maximizes the secret key rate. The magnitude of the optimal variance decreases as we increase the transmission distance. This means that increasing the amount of squeezing is not always helpful and there is an optimal squeezing at which the protocol displays its best performance.

Strategies such as SPS and displacement was utilized to enhance the maximum transmission distance or tolerance to channel loss [38–40]. Here, we revisit these strategies and consider optimization of state parameters that further enhances the performance. However, to our surprise, we found that SPS and displacement operation

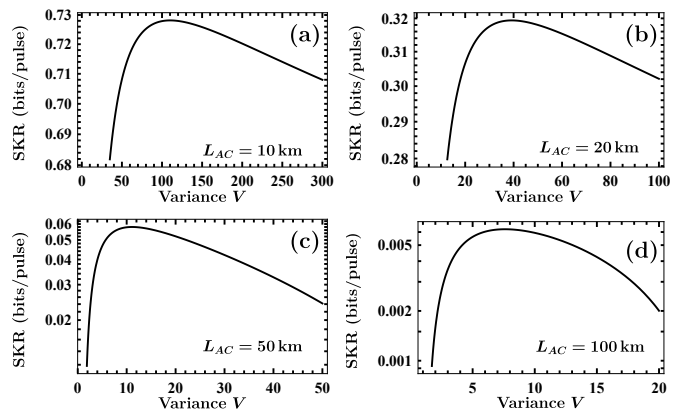


FIG. 2. Secret key rate (SKR) as a function of variance for different transmission distance L_{AC} for TMSV state based CV-MDI-QKD. We have assumed Charlie and Bob are at the same place, *i.e.*, $T_B = 1$. We have set the numerical values of the other parameters as $\beta = 96\%$, $T_B = 1$, $\epsilon_A^{\text{th}} = 19.09 \times 10^{-5} + 6.13 \times 10^{-5} \times L_{AC}$ and $\epsilon_B^{\text{th}} = 19.09 \times 10^{-5}$.

applied on Alice’s side are not advantageous in enhancing the tolerance to channel loss in CV-MDI-QKD.

The SPS-TMSC state depends on the variance V , displacement d , and the beam splitter transmissivity T_S involved in the implementation of the SPS [39, 40]. Setting $d = 0$ in the SPS-TMSC state, we obtain the SPS-TMSV state [38]. We optimize the secret key rate (3) over these state parameters, which could be succinctly expressed as

$$\begin{aligned} \max_{V, d, T_S} \quad & K(V, d, T_S) \\ \text{s.t.} \quad & 1 \leq V \leq 15, \\ & 0 \leq d \leq 5, \\ & 0 \leq T_S \leq 1. \end{aligned} \quad (4)$$

Here, we have put an upper limit of $V = 15$ on the vari-

¹ The numerical results of Ref. [38] are incorrect, which invalidates their conclusion regarding improved loss tolerance in CV-MDI-QKD using SPS-TMSV state.

ance of the original state². We show the optimized secret key rate as a function of transmission distance L_{AC} in Fig. 3.

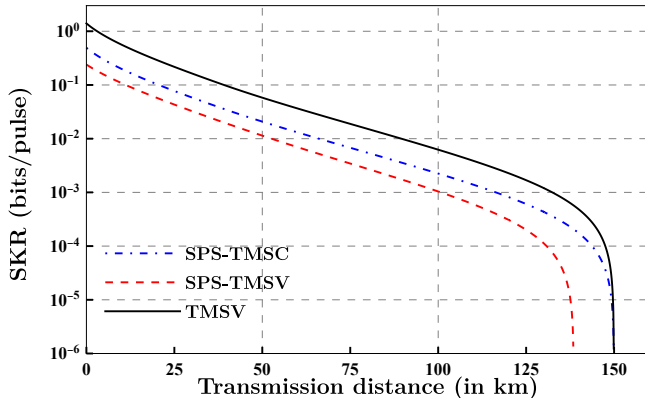


FIG. 3. Secret key rate (SKR) as a function of transmission distance L_{AC} . The SKR is optimized over the state parameters namely variance V , displacement d and the transmissivity T_S of the beam splitter involved in the SPS operation. We have set the numerical values of the other parameters as $\beta = 96\%$, $T_B = 1$, $\epsilon_A^{\text{th}} = 19.09 \times 10^{-5} + 6.13 \times 10^{-5} \times L_{AC}$ and $\epsilon_B^{\text{th}} = 19.09 \times 10^{-5}$.

We observe the tolerable channel loss for different states are in the following order:

$$\text{TMSV} \approx \text{SPS-TMSC} > \text{SPS-TMSV}. \quad (5)$$

The SPS-TMSV state can tolerate even less channel loss as compared to the TMSV state. The SPS-TMSC state, where displacement is coupled with SPS, can tolerate channel loss equal to the TMSV state. Therefore, the SPS operation implemented on Alice's side provides no advantage in CV-MDI-QKD at optimal parameters. Further, displacement also does not help in enhancing the tolerance to channel loss. These results are in stark contrast with Refs. [38–40], where SPS and displacement were claimed to enhance the loss tolerance. In Fig. 4, we show the variance, maximizing the secret key rate in the graphs depicted in Fig. 3.

The secret key rate is maximized at variance $V = 15$ for small transmission distances, aligning with the findings in Fig. 2 given the optimization constraint for variance (4). In the limit of maximal transmission distance, the optimal variance for both TMSV and SPS-TMSC states converges to $V \approx 6$. These squeezing variances are easily attainable in laboratory settings, leading to the conclusion that working with a TMSV state with a variance of $V \approx 6$ represents the most favorable choice for CV-MDI-QKD.

For the SPS-TMSC state, the optimal transmissivity is slightly below unity and exhibits slight variations. At

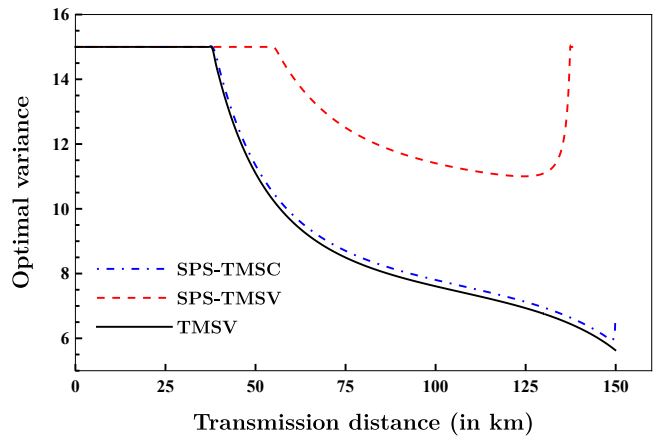


FIG. 4. Optimal variance V maximizing the secret key rate in Fig. 3.

a transmission distance of $L_{AC} = 25$ km, $T_S = 0.995$; at $L_{AC} = 125$ km, $T_S = 0.989$. For the SPS-TMSV state, the optimal transmissivity drops well below unity and shows significant variations as the transmission distance increases. Furthermore, the secret key rate is maximized at a displacement of $d = 5$ for almost the entire range of transmission distance, given the optimization constraint for displacement (4).

The advantage shown by SPS-TMSC state in Refs. [39, 40] is an artifact of working at high variance. To explicitly show this, we plot the transmission distance L_{AC} as a function of variance for a fixed secret key rate $K = 10^{-3}$ and show the result in Fig. 5. We note that Refs. [39, 40] showed the enhanced loss tolerance for SPS-TMSC state based CV-MDI-QKD at $V = 50$, $T_S = 0.9$, and $d = 2$.

Clearly, in the high variance regime (for instance, $V = 50$), the maximum transmission distance of the considered states in CV-MDI-QKD can be arranged in the following order:

$$\text{TMSV} < \text{SPS-TMSV} < \text{SPS-TMSC}, \quad (6)$$

which was precisely shown in Refs. [39, 40]. However, we notice that by working at $V \approx 6$, the performance of different states are in the following order:

$$\text{TMSV} \approx \text{SPS-TMSC} > \text{SPS-TMSV}. \quad (7)$$

This result further corroborates with our main result shown in Fig. 3. Therefore, analysis performed at non-optimal regime (high variance) in Refs. [39, 40] leads to an appearance of advantage with displacement and SPS. However, this advantage is merely apparent and not genuine.

Conclusion.— While earlier studies utilizing SPS and displacement CV-MDI-QKD have been conducted at fixed value of state parameters, we optimized the secret key rate over various state parameters with a view to optimize the performance and to obtain a global picture. Surprisingly, we discovered that neither SPS nor displacement offered any advantage in enhancing the loss tolerance of CV-MDI-QKD. The observed enhancement in

² Squeezed vacuum state with 15 dB squeezing ($V = 15.83$) has been demonstrated in lab [51].

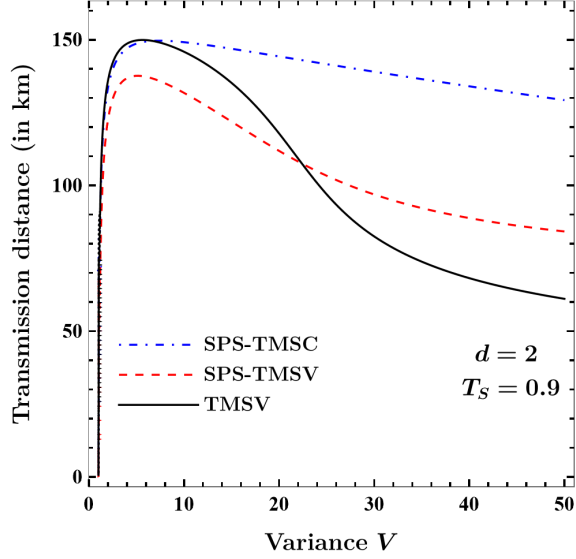


FIG. 5. Transmission distance L_{AC} as a function of variance for a fixed secret key rate $K = 10^{-3}$. We have set the numerical values of the other parameters as $\beta = 96\%$, $T_B = 1$, $\epsilon_A^{\text{th}} = 19.09 \times 10^{-5} + 6.13 \times 10^{-5} \times L_{AC}$ and $\epsilon_B^{\text{th}} = 19.09 \times 10^{-5}$.

the loss tolerance demonstrated for CV-MDI-QKD with the SPS-TMSC state could be attributed to operating at high variance, which is non-optimal [39, 40]. Moreover, the numerical results presented in Ref. [38] regarding CV-MDI-QKD with the SPS-TMSV state were found to be inaccurate, thereby refuting their assertion of enhanced loss tolerance through SPS. Our result will also impact similar studies in CV-MDI-QKD [41–43]. Therefore, our findings questions a commonly accepted notion within the field that SPS and displacement are beneficial in enhancing loss tolerance.

Our work raises numerous questions regarding the utility of non-Gaussian operations in CV quantum information processing, which is currently pursued by a large community of researchers. While we have focused on SPS by Alice, it is essential to also consider the scenario of SPS by Bob. While the utility of SPS in other CV-QKD protocols [35–37] needs to be properly re-assessed, the potential benefits of other non-Gaussian operations such as photon catalysis [40, 52, 53] and photon addition [40, 54] in CV-QKD also require critical examination. Since SPS has been shown to be useful in quantum teleportation [30–32] and quantum metrology [33, 34] our work call for a re-examination of these results from an optimality point of view.

Acknowledgement.— S.C. acknowledges the Prime Minister’s Research Fellowship (PMRF) scheme, GoI, for financial support. A. and C.K. acknowledge the financial support from **DST/ICPS/QuST/Theme-1/2019/General** Project number Q-68.

Appendix A: Calculation of the mutual information and Holevo bound

We start by computing the mutual information. We utilize the covariance matrix of the SPS-TMSC state to calculate the secret key rate, which is a lower bound of the secret key rate of the non-Gaussian state [55]. The covariance matrix of the SPS-TMSC state can be expressed in the following form:

$$\Sigma_{A_1 A'_2} = \begin{pmatrix} V_A^q & 0 & V_C^q & 0 \\ 0 & V_A^p & 0 & V_C^p \\ V_C^q & 0 & V_B^q & 0 \\ 0 & V_C^p & 0 & V_B^p \end{pmatrix}, \quad (\text{A1})$$

where $(\Sigma_{A_1 A'_2})_{ij} = \frac{1}{2} \langle \{\hat{\xi}_i, \hat{\xi}_j\} \rangle - \langle \hat{\xi}_i \rangle \langle \hat{\xi}_j \rangle$.

The covariance matrix representing the state of the modes $A_1 B'_1$ after interaction with the noisy channel can be written as [38]

$$\begin{aligned} \Sigma_{A_1 B'_1} &= \begin{pmatrix} V_A^q & 0 & \sqrt{T}V_C^q & 0 \\ 0 & V_A^p & 0 & \sqrt{T}V_C^p \\ \sqrt{T}V_C^q & 0 & T(V_B^q + \chi_{\text{ch}}) & 0 \\ 0 & \sqrt{T}V_C^p & 0 & T(V_B^p + \chi_{\text{ch}}) \end{pmatrix}, \\ &= \begin{pmatrix} \delta_1 & 0 & \kappa_1 & 0 \\ 0 & \delta_2 & 0 & \kappa_2 \\ \kappa_1 & 0 & \mu_1 & 0 \\ 0 & \kappa_2 & 0 & \mu_2 \end{pmatrix} = \begin{pmatrix} \Sigma_{A_1} & \Sigma_C \\ \Sigma_C & \Sigma_{B'_1} \end{pmatrix}. \end{aligned} \quad (\text{A2})$$

The covariance matrix of Alice is computed as follows after Bob performs heterodyne measurement:

$$\begin{aligned} \Sigma_{A_1|B'_1} &= \Sigma_{A_1} - \Sigma_C (\Sigma_{B'_1} + \mathbb{1}_2)^{-1} (\Sigma_C)^T, \\ &= \begin{pmatrix} \delta_1 - \frac{\kappa_1^2}{\mu_1 + 1} & 0 \\ 0 & \delta_2 - \frac{\kappa_2^2}{\mu_2 + 1} \end{pmatrix}. \end{aligned} \quad (\text{A3})$$

The classical mutual information is given by

$$I_{AB} = \frac{1}{2} \log_2 \left(\frac{\Sigma_{A_1}^q + 1}{\Sigma_{A_1|B'_1}^q + 1} \right) + \frac{1}{2} \log_2 \left(\frac{\Sigma_{A_1}^p + 1}{\Sigma_{A_1|B'_1}^p + 1} \right), \quad (\text{A4})$$

For the computation of the Holevo bound, we make the assumption that Eve possesses a purification of the state $\hat{\rho}_{A_1 B'_1 E F}$ and has access to Fred’s mode. The Holevo bound is then determined as follows:

$$\chi_{BE} = S(\hat{\rho}_{A_1 B'_1}) - S(\hat{\rho}_{A_1|B'_1}). \quad (\text{A5})$$

Here, $S(\hat{\rho})$ represents the von Neumann entropy associated with the state $\hat{\rho}$, and it is defined as follows:

$$S(\hat{\rho}) = \sum_i g(\nu_i), \quad (\text{A6})$$

where,

$$g(\nu) = \frac{\nu + 1}{2} \log_2 \left(\frac{\nu + 1}{2} \right) - \frac{\nu - 1}{2} \log_2 \left(\frac{\nu - 1}{2} \right). \quad (\text{A7})$$

Here, the symplectic eigenvalues of the covariance matrix of the state $\hat{\rho}$ are denoted as ν_i . The calculation of $S(\hat{\rho}_{A_1 B'_1})$ involves these symplectic eigenvalues obtained from the matrix in Eq. (A2), which are determined as follows:

$$\nu_{1,2} = \frac{1}{\sqrt{2}} \left[I_1 + I_2 + 2I_3 \pm \sqrt{(I_1 + I_2 + 2I_3)^2 - 4I_4} \right]^{1/2}, \quad (\text{A8})$$

where $I_1 = \delta_1 \delta_2$, $I_2 = \mu_1 \mu_2$, $I_3 = \kappa_1 \kappa_2$, and $I_4 = (\delta_1 \mu_1 - \kappa_1^2)(\delta_2 \mu_2 - \kappa_2^2)$. The computation of $S(\hat{\rho}_{A_1 B'_1})$ utilizes the symplectic eigenvalue extracted from the matrix provided in Eq. (A3), yielding the following result:

$$\nu_3 = \sqrt{\left(\delta_1 - \frac{\kappa_1^2}{\mu_1 + 1} \right) \left(\delta_2 - \frac{\kappa_2^2}{\mu_2 + 1} \right)}. \quad (\text{A9})$$

The secret key rate (3) can be calculated using the expressions of mutual information and Holevo bound.

-
- [1] N. Gisin, G. Ribordy, W. Tittel, and H. Zbinden, Quantum cryptography, *Rev. Mod. Phys.* **74**, 145 (2002).
- [2] V. Scarani, H. Bechmann-Pasquinucci, N. J. Cerf, M. Dušek, N. Lütkenhaus, and M. Peev, The security of practical quantum key distribution, *Rev. Mod. Phys.* **81**, 1301 (2009).
- [3] S. Pirandola, U. L. Andersen, L. Banchi, M. Berta, D. Bunandar, R. Colbeck, D. Englund, T. Gehring, C. Lupo, C. Ottaviani, J. L. Pereira, M. Razavi, J. S. Shaari, M. Tomamichel, V. C. Usenko, G. Vallone, P. Villoresi, and P. Wallden, Advances in quantum cryptography, *Adv. Opt. Photon.* **12**, 1012 (2020).
- [4] C. H. Bennett and G. Brassard, Proceedings of the IEEE international conference on computers, systems and signal processing (IEEE Press, 1984, New York, 1984) pp. 175–179.
- [5] A. K. Ekert, Quantum cryptography based on bell's theorem, *Phys. Rev. Lett.* **67**, 661 (1991).
- [6] C. H. Bennett, F. Bessette, G. Brassard, L. Salvail, and J. Smolin, Experimental quantum cryptography, *Journal of Cryptology* **5**, 3 (1992).
- [7] J.-Y. Wang, B. Yang, S.-K. Liao, L. Zhang, Q. Shen, X.-F. Hu, J.-C. Wu, S.-J. Yang, H. Jiang, Y.-L. Tang, B. Zhong, H. Liang, W.-Y. Liu, Y.-H. Hu, Y.-M. Huang, B. Qi, J.-G. Ren, G.-S. Pan, J. Yin, J.-J. Jia, Y.-A. Chen, K. Chen, C.-Z. Peng, and J.-W. Pan, Direct and full-scale experimental verifications towards ground-satellite quantum key distribution, *Nature Photonics* **7**, 387 (2013).
- [8] T. C. Ralph, Continuous variable quantum cryptography, *Phys. Rev. A* **61**, 010303 (1999).
- [9] M. Hillery, Quantum cryptography with squeezed states, *Phys. Rev. A* **61**, 022309 (2000).
- [10] N. J. Cerf, M. Lévy, and G. V. Assche, Quantum distribution of gaussian keys using squeezed states, *Phys. Rev. A* **63**, 052311 (2001).
- [11] F. Grosshans and P. Grangier, Continuous variable quantum cryptography using coherent states, *Phys. Rev. Lett.* **88**, 057902 (2002).
- [12] F. Grosshans, G. Van Assche, J. Wenger, R. Brouri, N. J. Cerf, and P. Grangier, Quantum key distribution using gaussian-modulated coherent states, *Nature* **421**, 238 (2003).
- [13] C. Weedbrook, S. Pirandola, R. García-Patrón, N. J. Cerf, T. C. Ralph, J. H. Shapiro, and S. Lloyd, Gaussian quantum information, *Rev. Mod. Phys.* **84**, 621 (2012).
- [14] F. Laudenbach, C. Pacher, C.-H. F. Fung, A. Poppe, M. Peev, B. Schrenk, M. Hentschel, P. Walther, and H. Hübel, Continuous-variable quantum key distribution with gaussian modulation—the theory of practical implementations, *Advanced Quantum Technologies* **1**, 1800011 (2018).
- [15] J. Barrett, L. Hardy, and A. Kent, No signaling and quantum key distribution, *Phys. Rev. Lett.* **95**, 010503 (2005).
- [16] A. Acín, N. Brunner, N. Gisin, S. Massar, S. Pironio, and V. Scarani, Device-independent security of quantum cryptography against collective attacks, *Phys. Rev. Lett.* **98**, 230501 (2007).
- [17] S. L. Braunstein and S. Pirandola, Side-channel-free quantum key distribution, *Phys. Rev. Lett.* **108**, 130502 (2012).
- [18] H.-K. Lo, M. Curty, and B. Qi, Measurement-device-independent quantum key distribution, *Phys. Rev. Lett.* **108**, 130503 (2012).
- [19] S. Pirandola, C. Ottaviani, G. Spedalieri, C. Weedbrook, S. L. Braunstein, S. Lloyd, T. Gehring, C. S. Jacobsen, and U. L. Andersen, High-rate measurement-device-independent quantum cryptography, *Nature Photonics* **9**, 397 (2015).
- [20] Z. Li, Y.-C. Zhang, F. Xu, X. Peng, and H. Guo, Continuous-variable measurement-device-independent quantum key distribution, *Phys. Rev. A* **89**, 052301 (2014).
- [21] X.-C. Ma, S.-H. Sun, M.-S. Jiang, M. Gui, and L.-M. Liang, Gaussian-modulated coherent-state measurement-device-independent quantum key distribution, *Phys. Rev. A* **89**, 042335 (2014).
- [22] G. Adesso and F. Illuminati, Entanglement in continuous-variable systems: recent advances and current perspectives, *J. Phys. A* **40**, 7821 (2007).
- [23] G. Adesso, S. Ragy, and A. R. Lee, Continuous variable quantum information: Gaussian states and beyond, *Open Syst. Inf. Dyn.* **21**, 1440001, 47 (2014).
- [24] M. Walschaers, Non-gaussian quantum states and where to find them, *PRX Quantum* **2**, 030204 (2021).
- [25] J. Fiurášek, Gaussian transformations and distillation of entangled gaussian states, *Phys. Rev. Lett.* **89**, 137904 (2002).
- [26] G. Giedke and J. Ignacio Cirac, Characterization of gaussian operations and distillation of gaussian states, *Phys. Rev. A* **66**, 032316 (2002).
- [27] J. Eisert, S. Scheel, and M. B. Plenio, Distilling gaussian states with gaussian operations is impossible, *Phys. Rev. Lett.* **89**, 137903 (2002).
- [28] S. Lloyd and S. L. Braunstein, Quantum computation over continuous variables, *Phys. Rev. Lett.* **82**, 1784 (1999).

- [29] S. D. Bartlett and B. C. Sanders, Universal continuous-variable quantum computation: Requirement of optical nonlinearity for photon counting, *Phys. Rev. A* **65**, 042304 (2002).
- [30] T. Opatrny, G. Kurizki, and D.-G. Welsch, Improvement on teleportation of continuous variables by photon subtraction via conditional measurement, *Phys. Rev. A* **61**, 032302 (2000).
- [31] F. Dell'Anno, S. De Siena, L. Albano, and F. Illuminati, Continuous-variable quantum teleportation with non-gaussian resources, *Phys. Rev. A* **76**, 022301 (2007).
- [32] C. Kumar and S. Arora, Success probability and performance optimization in non-gaussian continuous-variable quantum teleportation, *Phys. Rev. A* **107**, 012418 (2023).
- [33] R. Carranza and C. C. Gerry, Photon-subtracted two-mode squeezed vacuum states and applications to quantum optical interferometry, *J. Opt. Soc. Am. B* **29**, 2581 (2012).
- [34] C. Kumar, Rishabh, and S. Arora, Realistic non-gaussian-operation scheme in parity-detection-based mach-zehnder quantum interferometry, *Phys. Rev. A* **105**, 052437 (2022).
- [35] Y. Guo, Q. Liao, Y. Wang, D. Huang, P. Huang, and G. Zeng, Performance improvement of continuous-variable quantum key distribution with an entangled source in the middle via photon subtraction, *Phys. Rev. A* **95**, 032304 (2017).
- [36] P. Huang, G. He, J. Fang, and G. Zeng, Performance improvement of continuous-variable quantum key distribution via photon subtraction, *Phys. Rev. A* **87**, 012317 (2013).
- [37] Z. Li, Y. Zhang, X. Wang, B. Xu, X. Peng, and H. Guo, Non-gaussian postselection and virtual photon subtraction in continuous-variable quantum key distribution, *Phys. Rev. A* **93**, 012310 (2016).
- [38] H.-X. Ma, P. Huang, D.-Y. Bai, S.-Y. Wang, W.-S. Bao, and G.-H. Zeng, Continuous-variable measurement-device-independent quantum key distribution with photon subtraction, *Phys. Rev. A* **97**, 042329 (2018).
- [39] C. Kumar, J. Singh, S. Bose, and Arvind, Coherence-assisted non-gaussian measurement-device-independent quantum key distribution, *Phys. Rev. A* **100**, 052329 (2019).
- [40] J. Singh and S. Bose, Non-gaussian operations in measurement-device-independent quantum key distribution, *Phys. Rev. A* **104**, 052605 (2021).
- [41] Y. Zhao, Y. Zhang, B. Xu, S. Yu, and H. Guo, Continuous-variable measurement-device-independent quantum key distribution with virtual photon subtraction, *Phys. Rev. A* **97**, 042328 (2018).
- [42] Y.-H. Zhou, S.-F. Qin, W.-M. Shi, and Y.-G. Yang, Continuous variable measurement-device-independent quantum key distribution based on photon subtraction and optical amplifiers, *Optik* **242**, 166826 (2021).
- [43] Y. Wang, S. Zou, Y. Mao, and Y. Guo, Improving underwater continuous-variable measurement-device-independent quantum key distribution via zero-photon catalysis, *Entropy* **22**, 10.3390/e22050571 (2020).
- [44] S. Olivares, Quantum optics in the phase space, *The European Physical Journal Special Topics* **203**, 3 (2012).
- [45] F. Grasselli, Beyond point-to-point quantum key distribution, in *Quantum Cryptography: From Key Distribution to Conference Key Agreement* (Springer International Publishing, Cham, 2021) pp. 83–104.
- [46] Y. Zhang, Z. Chen, S. Pirandola, X. Wang, C. Zhou, B. Chu, Y. Zhao, B. Xu, S. Yu, and H. Guo, Long-distance continuous-variable quantum key distribution over 202.81 km of fiber, *Phys. Rev. Lett.* **125**, 010502 (2020).
- [47] C. Ottaviani, G. Spedalieri, S. L. Braunstein, and S. Pirandola, Continuous-variable quantum cryptography with an untrusted relay: Detailed security analysis of the symmetric configuration, *Phys. Rev. A* **91**, 022320 (2015).
- [48] F. Grosshans, N. J. Cerf, J. Wenger, R. Tualle-Broui, and P. Grangier, Virtual entanglement and reconciliation protocols for quantum cryptography with continuous variables, *Quantum Info. Comput.* **3**, 535–552 (2003).
- [49] C. Weedbrook, A. M. Lance, W. P. Bowen, T. Symul, T. C. Ralph, and P. K. Lam, Quantum cryptography without switching, *Phys. Rev. Lett.* **93**, 170504 (2004).
- [50] I. Devetak and A. Winter, Distillation of secret key and entanglement from quantum states, *Proceedings of the Royal Society A: Mathematical, Physical and Engineering Sciences* **461**, 207 (2005).
- [51] H. Vahlbruch, M. Mehmet, K. Danzmann, and R. Schnabel, Detection of 15 db squeezed states of light and their application for the absolute calibration of photoelectric quantum efficiency, *Phys. Rev. Lett.* **117**, 110801 (2016).
- [52] Y. Guo, W. Ye, H. Zhong, and Q. Liao, Continuous-variable quantum key distribution with non-gaussian quantum catalysis, *Phys. Rev. A* **99**, 032327 (2019).
- [53] H. Zhong, Y. Guo, Y. Mao, W. Ye, and D. Huang, Virtual zero-photon catalysis for improving continuous-variable quantum key distribution via gaussian post-selection, *Scientific Reports* **10**, 17526 (2020).
- [54] J. Huang, W. Ye, C. Liu, Q. Kuang, and F. Jia, Underwater quantum key distribution with continuous-variable via photon additions, *Results in Physics* **54**, 107136 (2023).
- [55] R. García-Patrón and N. J. Cerf, Unconditional optimality of gaussian attacks against continuous-variable quantum key distribution, *Phys. Rev. Lett.* **97**, 190503 (2006).